Structure of Diethyl Phosphate Bound to the Binuclear Metal Center of Phosphotriesterase[†,‡]

Jungwook Kim,[§] Ping-Chuan Tsai,[||] Shi-Lu Chen,[⊥] Fahmi Himo,*[,⊥] Steven C. Almo,*[,§] and Frank M. Raushel*[,||]

Albert Einstein College of Medicine, 1300 Morris Park Avenue, Bronx, New York 10461, Department of Chemistry, P.O. Box 30012, Texas A&M University, College Station, Texas 77842-3012, and Department of Theoretical Chemistry, School of Biotechnology, Royal Institute of Technology, 10691 Stockholm, Sweden

Received May 22, 2008; Revised Manuscript Received July 22, 2008

ABSTRACT: The bacterial phosphotriesterase (PTE) from *Pseudomonas diminuta* catalyzes the hydrolysis of organophosphate esters at rates close to the diffusion limit. X-ray diffraction studies have shown that a binuclear metal center is positioned in the active site of PTE and that this complex is responsible for the activation of the nucleophilic water from solvent. In this paper, the three-dimensional structure of PTE was determined in the presence of the hydrolysis product, diethyl phosphate (DEP), and a product analogue, cacodylate. In the structure of the PTE−diethyl phosphate complex, the DEP product is found symmetrically bridging the two divalent cations. The DEP displaces the hydroxide from solvent that normally bridges the two divalent cations in structures determined in the presence or absence of substrate analogues. One of the phosphoryl oxygen atoms in the PTE−DEP complex is 2.0 Å from the α-metal ion, while the other oxygen is 2.2 Å from the β-metal ion. The two metal ions are separated by a distance of 4.0 Å. A similar structure is observed in the presence of cacodylate. Analogous complexes have previously been observed for the product complexes of isoaspartyl dipeptidase, D-aminoacylase, and dihydroorotase from the amidohydrolase superfamily of enzymes. The experimentally determined structure of the PTE−diethyl phosphate product complex is inconsistent with a recent proposal based upon quantum mechanical/molecular mechanical simulations which postulated the formation of an asymmetrical product complex bound exclusively to the β-metal ion with a metal−metal separation of 5.3 Å. This structure is also inconsistent with a chemical mechanism for substrate hydrolysis that utilizes the bridging hydroxide as a base to abstract a proton from a water molecule loosely associated with the α-metal ion. Density functional theory (DFT) calculations support a reaction mechanism that utilizes the bridging hydroxide as the direct nucleophile in the hydrolysis of organophosphate esters by PTE.

The amidohydrolase superfamily (AHS)[1] of enzymes catalyzes hydrolytic, decarboxylation, isomerization, and hydration reactions within carbohydrate-, nucleic acid-, and amino acid-based substrates (*1*). Most of the structurally characterized enzymes of the AHS contain either a binuclear or mononuclear metal center embedded at the C-terminal end of a $(\beta/\alpha)_8$-barrel structural domain. For those enzymes that catalyze hydrolytic reactions, the metal centers have been shown to activate solvent water for nucleophilic attack. High-resolution X-ray structures have been obtained for approximately 20 members of the AHS, and in these enzymes, the metal centers are naturally populated by zinc, iron, or nickel (*1*). In addition, some members of the AHS are also active with manganese, cobalt, or cadmium (*2*). Perhaps the best-characterized member of the amidohydrolase superfamily is the bacterial phosphotriesterase from *Pseudomonas diminuta* (*3*).

Phosphotriesterase (PTE) catalyzes the hydrolysis of a wide range of organophosphate esters, including agricultural pesticides and highly toxic chemical warfare agents (*3*−*5*). A natural substrate for PTE is not known; however, the purified PTE exhibits a remarkable catalytic activity toward the hydrolysis of the commercial pesticide, paraoxon. Kinetic constants k_{cat} and k_{cat}/K_m of 10^4 s^{-1} and 10^8 M^{-1} s^{-1}, respectively, have been measured for the hydrolysis of this substrate (*6, 7*). The reaction for the hydrolysis of paraoxon is presented in Scheme 1. The enzyme has been crystallized, and high-resolution X-ray structures of the Zn/Zn−, Cd/Cd−, Mn/Mn−, and Zn/Cd−PTE have been determined (*2*). Shown in Figure 1 is the coordination scheme for the binuclear metal center of Cd/Cd−PTE. The more solvent-shielded metal (M_α) is coordinated to His-55, His-57, and Asp-301, whereas the more solvent-exposed metal (M_β) is coordinated to His-201, His-230, and two water molecules

[†] This work was supported in part by the NIH (Grants GM71790 and GM68550) and the Robert A. Welch Foundation (Grant A-840). J.K. was supported by Grant GM76988. F.H. acknowledges financial help from The Swedish National Research Council and The Carl Trygger Foundation.

[‡] The X-ray coordinates and structure factors have been deposited in the Protein Data Bank as entries 2O4Q and 3CAK.

* To whom correspondence should be addressed. F.M.R.: telephone, (979) 845-3373; fax, (979) 845-9452; e-mail, raushel@tamu.edu. S.C.A.: telephone, (718) 430-2746; fax, (718) 430-8565; e-mail, almo@aecom.yu.edu. F.H.: telephone, 46-8-55378415; fax, 46-8-55378590; e-mail, himo@theochem.kth.se.

[§] Albert Einstein College of Medicine.

[||] Texas A&M University.

[⊥] Royal Institute of Technology.

[1] Abbreviations: AHS, amidohydrolase superfamily; DFT, density functional theory; PTE, phosphotriesterase; DEP, diethyl phosphate.

10.1021/bi800971v CCC: $40.75
Published on Web 08/15/2008

Scheme 1

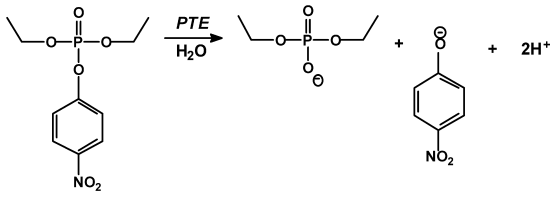

from the solvent. The two metals are bridged to one another by a carboxylated lysine (Lys-169) and hydroxide. The bridging hydroxide is additionally hydrogen bonded to the side chain carboxylate of Asp-301.

The reaction mechanism for the hydrolysis of organophosphate triesters by phosphotriesterase has received considerable experimental and computational attention (*8*−*11*). Presented in Scheme 2 is a slightly modified reaction mechanism, originally proposed by Aubert et al., for the hydrolysis of paraoxon by the phosphotriesterase from *P. diminuta* (*8*). In this mechanism, the organophosphate substrate binds to the active site with the displacement of a water molecule from the β-metal ion. The interaction of the substrate with the β-metal ion weakens the coordination of the bridging hydroxide to the β-metal ion and facilitates the nucleophilic attack of the hydroxide in an S_N2-like reaction on the phosphorus center of the substrate. The bond to the leaving group phenol is broken, and the single proton from the nucleophilic hydroxide is transferred to Asp-301. The anionic diethyl phosphate is bound within the active site as a bridging ligand between the two divalent cations. The diethyl phosphate dissociates from the active site, and the binuclear metal center is subsequently recharged for another round of catalysis.

Experimental evidence of the direct interaction of the substrate with the β-metal ion comes from the X-ray structure of PTE bound with a diisopropyl methyl phosphonate inhibitor (PDB entry 1EZ2) and the differential effects on the kinetic constants for the hydrolysis of phosphate and thiophosphate esters with zinc- and cadmium-substituted variants of PTE (*8*). Support for the weakening of the interaction of the bridging hydroxide with the β-metal ion is derived from the loss of antiferromagnetic coupling between the two metal ions in Mn/Mn−PTE upon binding of substrate analogues using EPR spectroscopy (*12*). The utilization of the hydroxide that is bridging the two metal ions as the direct nucleophile is supported by the observation that in the presence of substrate analogues there are no other

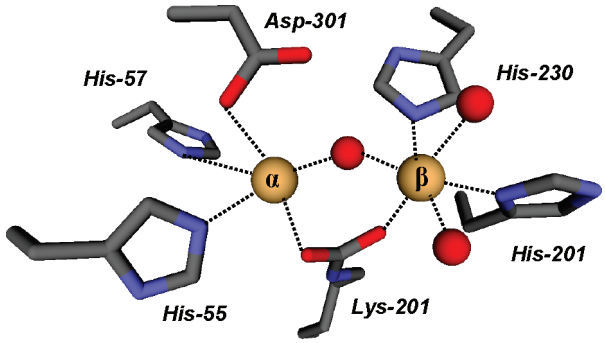

FIGURE 1: Model for the structure of the binuclear metal center within the active site of the Cd/Cd−PTE hybrid (*2*). The coordinates were taken from PDB entry 1JGM. The two metal ions are depicted as light brown spheres.

water molecules bound to either of the two metal ions in Zn/Zn−PTE.

General support for the reaction mechanism depicted in Scheme 2 was also provided by recent density functional theory (DFT) calculations by Chen et al. (*9*). A model of the PTE active site was devised on the basis of the crystal structure of the wild-type Zn/Zn enzyme (PDB entry 1HZY). The calculations showed that the bridging hydroxide is sufficiently nucleophilic to attack the phosphorus center of organophosphate triester substrates.

Recently, two provocative modifications to the mechanism presented in Scheme 2 have been proposed (*10, 11*). In a computational assessment of the PTE reaction mechanism, Wong and Gao have postulated a mononuclear coordination scheme of protonated diethyl phosphate to the β-metal ion that is coupled with a lengthening of the metal−metal distance from 3.6 to 5.3 Å as the reaction proceeds from an enzyme−substrate complex to an enzyme−product complex (*10*). A representation of this product complex is provided in Scheme 3. In addition, Ollis and colleagues have proposed that the bridging hydroxide acts not as a nucleophile but as a base in the abstraction of a proton from a water molecule that is apparently loosely coordinated to the α-metal ion. The chemical mechanism and product complex proposed by Ollis and colleagues are illustrated in Scheme 3 (*11*). Experimental support for this proposal derives primarily from an X-ray structure of a dimethyl thiophosphate complex of the PTE from *Agrobacterium radiobacter* and catalytic properties of model complexes that are purported to mimic the active site of PTE (*13*).

In this investigation, we have utilized X-ray diffraction techniques to probe the structure of diethyl phosphate bound to the active site of PTE. This structure has been used to help differentiate among the three mechanistic possibilities for the hydrolysis of organophosphate esters by PTE. In addition, we have performed DFT calculations to assess the energetic feasibility of the base mechanism proposed by Ollis and co-workers.

MATERIALS AND METHODS

Purification of the Wild Type and G60A Mutant. The genes encoding wild-type PTE and the G60A mutant were ligated between the *Nde*I and *Eco*RI sites of a pET20b(+) plasmid. The wild-type and mutant plasmids were transformed into *Escherichia coli* strain BL-21(DE3) cells (*7*). The transformed BL-21(DE3) cells were inoculated in Luria-Bertani (LB) broth overnight at 37 °C. The overnight cultures were then incubated in Terrific Broth (TB) containing 100 μg/mL ampicillin and 1.0 mM $CoCl_2$ at 30 °C. IPTG was added when the OD_{600} reached 0.4, followed by incubation for 36−42 h at 30 °C which allowed the reaction to reach the stationary phase. The cell paste was harvested by centrifugation at 4 °C. The wild-type PTE and G60A mutant were purified as previously described (*8*). SDS−polyacrylamide gel electrophoresis demonstrated that wild-type PTE and the G60A mutant migrated with proteins having a molecular mass of ~36 kDa. The purity was estimated to be >95%.

Measurement of Kinetic Constants. The kinetic parameters were obtained by fitting the data to eq 1

$$v/E_t = k_{cat}[A]/(K_a + [A]) \quad (1)$$

Scheme 2

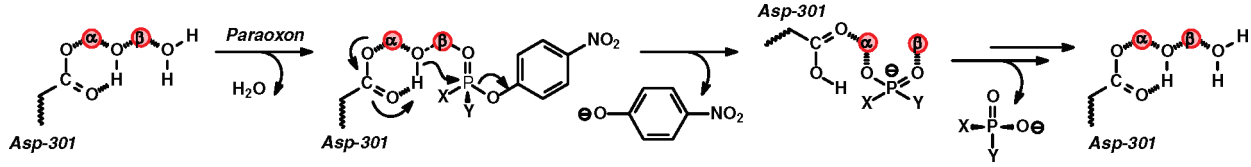

Scheme 3

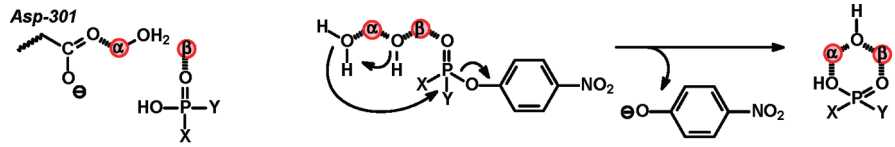

where v is the initial velocity, k_{cat} is the turnover number, [A] is the substrate concentration, E_t is the enzyme concentration, and K_a is the Michaelis constant. The inhibition constants, K_{ii} and K_{is}, for the noncompetitive inhibition of cacodylate in the presence of the substrate paraoxon were determined by fitting the data to eq 2

$$v/E_t = k_{cat}[A]/[K_a(1 + [I]/K_{is}) + [A](1 + [I]/K_{ii})] \quad (2)$$

where [I] is the concentration of inhibitor and the other constants have been defined previously. The concentration of paraoxon was varied from 0.05 to 2.5 mM. Six different cacodylate concentrations were used in these assays, ranging from 0 to 250 mM. The rate was measured by following the change in absorbance at 400 nm.

Synthesis of Diethyl Phosphate. Diethyl phosphate was synthesized by Y. Li of Texas A&M University. Diethyl phosphorochloridate was reacted with phenol in ethyl ether in the presence of triethylamine to yield diethyl phenyl phosphate after purification using silica gel chromatography. Hydrogenation of the resulting organophosphate in methanol using Pd/C as a catalyst provided diethyl hydrogen phosphate quantitatively after separation of the catalyst by filtration and removal of the solvent by evaporation under reduced pressure (*14*). The identity and the purity (>98%) of the diethyl phosphate were confirmed by ^{1}H and ^{31}P NMR spectroscopy.

X-ray Structure Determination and Refinement. The G60A mutant was crystallized by hanging drop vapor diffusion at 21 °C by mixing 1 μL of the protein with 1 μL of reservoir solution [0.2 M magnesium acetate, 0.1 M sodium cacodylate (pH 6.5), and 20% polyethylene glycol (PEG 8000)] and equilibrating over 1.0 mL of reservoir solution. X-ray data were collected on a MAR CCD 165 mm detector at the NSLS X3A beamline, using an X-ray wavelength at 0.97904 Å, and processed with HKL2000 (*15*). The G60A crystal exhibited diffraction consistent with space group P_1 (a = 55.29 Å, b = 68.30 Å, c = 90.03 Å, α = 90.05°, β = 100.42°, and γ = 89.96°). There were four G60A molecules (two homodimers) in the asymmetric unit.

The wild-type Co/Co−PTE was cocrystallized with 17 mM diethyl phosphate (DEP) in 0.1 M Bis-Tris (pH 6.5) and 20% PEG monomethyl ether 5000. X-ray data were collected on an R-Axis IV^{++} image plate detector using Cu Kα radiation from a Rigaku RU-H3R X-ray generator and processed using HKL2000 (*15*). The cocrystals of wild-type PTE with DEP exhibit diffraction consistent with space group P_1 (a = 43.29 Å, b = 45.34 Å, c = 78.91 Å, α = 104.73°, β = 93.40°, and γ = 97.65°). Two protein molecules were observed in the asymmetric unit.

Table 1: Data Collection and Refinement Statistics

	G60A−cacodylate	wild-type PTE−DEP
Data Collection		
resolution (Å)	31.64−1.95	20.49−1.83
no. of observed reflections	270828	137406
no. of unique reflections	91515	47158
completeness	96.3 (80.7)[a]	93.2 (81.8)[a]
I/σ	15.8 (3.4)[a]	13.2 (3.0)[a]
R_{merge}[b]	0.076 (0.286)[a]	0.061 (0.319)[a]
Refinement		
no. of protein non-hydrogen atoms	10161	5116
no. of water molecules	1163	843
R_{cryst}[c]	0.167	0.140
R_{free}[c]	0.224	0.196
average B-factor (Å^2)		
main chain	20.5	13.1
side chains	22.2	15.2
waters	30.6	27.6
rmsd from ideal geometry		
bond lengths (Å)	0.014	0.014
bond angles (deg)	1.5	1.4

[a] Values in parentheses correspond to the highest-resolution shell (2.02−1.95 Å for G60A and 1.90−1.83 Å for wild-type PTE with DEP). [b] $R_{merge} = \sum\sum_j|I_j(hkl) - \langle I(hkl)\rangle|/\sum\sum_j|\langle I(hkl)\rangle|$, where I_j is the intensity measurement for reflection j and $\langle I\rangle$ is the mean intensity over j reflections. [c] R_{cryst} (R_{free}) $= \sum||F_{obs}(hkl)| - |F_{calc}(hkl)||/\sum|F_{obs}(hkl)|$, where F_{obs} and F_{calc} are observed and calculated structure factors, respectively. No σ cutoff was applied. Five percent of the reflections were excluded from the refinement and used to calculate R_{free}.

The structures of G60A and wild-type PTE with bound DEP were determined by molecular replacement using MOLREP with 1P6B and 2OB3 as initial search models, respectively (*16*). Solvent water molecules were built using Arp/wArp (*17*). All subsequent model building and refinement was carried out with Coot (*18*) and REFMAC5 (*19*). The final models were refined to 1.95 with R_{work} and R_{free} values of 0.167 and 0.224, respectively, and to 1.83 Å with values of 0.140 and 0.196, respectively (Table 1).

Computational Details. All theoretical calculations were performed using the hybrid density functional theory (DFT) B3LYP (*20*−*22*). Geometry optimization was carried out with the 6-31G(d,p) basis set for all elements except Zn, for which the effective core potential LANL2DZ basis set was used. On the basis of these geometries, more accurate energies were obtained by performing single-point calculations with the larger 6-311+G(2d,2p) basis set for all

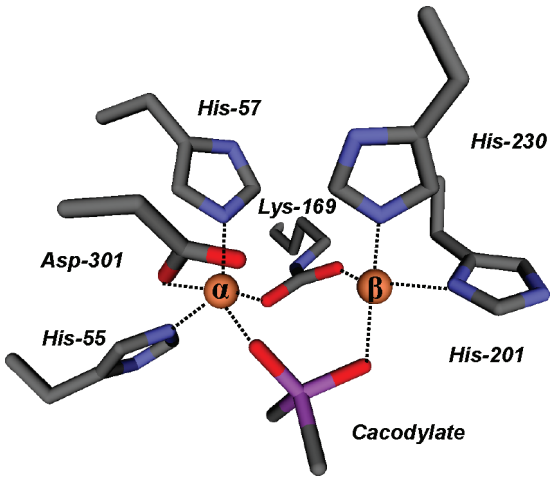

FIGURE 2: Model for the active site of the Co/Co−PTE hybrid (mutant G60A) obtained from crystals grown in the presence of cacodylate.

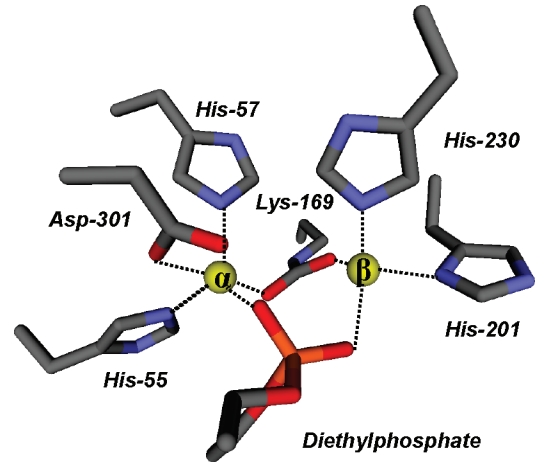

FIGURE 3: Model for the active site of the wild-type Co/Co−PTE hybrid from crystals grown in the presence of diethyl phosphate.

elements. Solvation effects were calculated at the same level of theory as the optimizations by performing single-point calculations on the optimized structures using the CPCM method (*23*−*26*). The dielectric constant (ε) was set to 4. Frequency calculations were performed at the same level of theory as the optimizations to obtain zero-point energies (ZPE) and to confirm the nature of the stationary points. All calculations were performed using Gaussian03 (*27*).

RESULTS

Inhibition by Cacodylate. The kinetic constants k_{cat}, k_{cat}/K_a, and K_a for the hydrolysis of paraoxon by Co/Co−G60A at pH 9.0 are 2900 s^{-1}, 1.34 × 10^7 M^{-1} s^{-1}, and 210 μM, respectively. The inhibition of Co/Co−G60A was assessed using cacodylate as an inhibitor of paraoxon hydrolysis. The double-reciprocal plots (data not shown) intersect to the left of the vertical axis, and thus, cacodylate is a noncompetitive inhibitor versus paraoxon. The kinetic inhibition constants, K_{is} and K_{ii}, determined from fits of the data to eq 2, are 260 ± 100 and 110 ± 10 mM, respectively.

Structure of G60A with Cacodylate. The crystals of G60A contain two homodimers in the asymmetric unit. As expected, two metal atoms were found in the active site for each monomer; however, an additional strong feature in the electron density was observed close to the binuclear metal center in all subunits during the refinement. The tetrahedral electron density appeared to interact directly with both metal atoms and was consistent with cacodylate, which was present in the crystallization solution (Figure S1 of the Supporting Information). The average *B*-factors for the main chain protein atoms and cacodylate are 20.52 and 20.70 $Å^2$, respectively. Cacodylate is bound to both metal ions with average distances of 1.98 ± 0.03 and 2.07 ± 0.06 Å to the α- and β-metal, respectively. The α-metal ion is coordinated to His-55, His-57, and Asp-301, whereas the β-metal ion is coordinated to His-201 and His-230. An image of these interactions is presented in Figure 2. The cacodylate ligand has replaced the bridging hydroxide that has been observed in a number of PTE structures (*2*). No water molecules are observed to interact with either metal ion in any of the four molecules in the asymmetric unit of the G60A structure. In addition to the two metal ions, cacodylate is within hydrogen bonding distance of Trp-131, the carboxylated Lys-169, His-201, and Asp-301.

Structure of Wild-Ttype PTE with Diethyl Phosphate. Diethyl phosphate (DEP) is the hydrolysis product of paraoxon, the best known substrate for PTE. Various concentrations of DEP, as high as 100 mM, were tested for cocrystallization with wild-type PTE before an optimized condition was determined. In the cocrystals, electron density for DEP was unambiguously located around the binuclear metal site in one subunit (Figure S2A of the Supporting Information). However, the lack of electron density corresponding to one of the two ethyl groups within the ligand was observed in the second subunit (Figure S2B of the Supporting Information). The electron density was modeled as monoethyl phosphate during the refinement for this subunit. The phosphoryl oxygen atom which is not coordinated to either metal is relatively solvent exposed, and the ethyl group occupies a more buried hydrophobic pocket. Subsequent NMR experiments showed that the initial concentration of monoethyl phosphate in the sample of diethyl phosphate was negligible (<1%), and the enzymatic hydrolysis of DEP by PTE was beyond the detection limit even after incubation of PTE with DEP for 5 days (data not shown). These observations suggest that the ethyl group of the second DEP is not observed due to disorder.

With the exception of the missing ethyl group, both ligands of DEP bind in a very similar manner within the binuclear metal center. Therefore, the following discussion will refer only to the first subunit that contains the fully modeled DEP. One of the ethyl groups orients toward a hydrophobic patch, composed of Gly-60, Ile-106, Trp-131, and Leu-303. The other ethyl group is more solvent exposed and forms hydrogen bonds through the phosphate ester oxygen with two water molecules. One of the phosphoryl oxygen atoms of DEP is 1.97 Å from α-metal ion, while the other oxygen is 2.17 Å from the β-metal. The orientation of diethyl phosphate within the active site of PTE is presented in Figure 3. These distances are similar to the orientation of cacodylate in the G60A PTE structure. Moreover, there is no bridging water observed in the binuclear metal site, as a result of the complete displacement by DEP. The DEP ligand is near $N_{\varepsilon 1}$ of Trp-131, the carboxylate oxygen atoms of the carboxylated Lys-169, and the carboxylate oxygen atoms of Asp-301. $N_{\delta 1}$ of His-201 is slightly farther from DEP (3.39 Å) in the

structure of the wild-type enzyme than from cacodylate (3.19 Å) in the G60A structure.

DFT Calculations. To further examine the feasibility of the base mechanism proposed by Ollis and co-workers (*11*), we have performed DFT calculations using the same model of the Zn/Zn−enzyme active site as in the previous calculations (*9*). The model is based on the high-resolution crystal structure of the wild-type Zn/Zn−PTE from *P. diminuta* (PDB entry 1HZY) and consists of the two zinc ions and their first-shell ligands, including the bridging hydroxide, the four histidines (His-55, His-57, His-201, and His-230), Asp-301, and the carboxylated Lys-169. Hydrogen atoms were added manually, and the ligands were truncated so that only side chains were kept in the model. The histidines were thus represented by imidazoles, and the aspartate was represented by an acetate and the carboxylated lysine by a carboxylated methylamine (see Figure 4). Dimethyl 4-nitrophenyl phosphate was chosen as a model substrate, as in the previous study (*9*). The water molecule, postulated to be the nucleophile in the base mechanism, was added to the model. The model thus consists of 85 atoms and has a total charge of +1.

In the reactant species (Figure 4, React), the phosphoryl oxygen of the substrate binds to the more solvent-exposed β-Zn site and the leaving group is located at the position opposite the bridging hydroxide. According to the base proposal, the nucleophilic water molecule is bound to the α-Zn. In the calculations, we first placed the water molecule there, but we could not locate a stable conformation with the water bound to the α-Zn. Instead, it dissociates from the Zn during the optimization and forms a hydrogen bond to the bridging hydroxide (see Figure 4, React). From these calculations, we can thus conclude that a hexacoordinate α-Zn is quite unlikely.

We have furthermore optimized the transition state for the nucleophilic attack with the bridging hydroxide acting as a base. The optimized structure is displayed in Figure 4 with important distances indicated. The critical distance between the water oxygen and the phosphorus center (O_W−P) is 1.99 Å. Simultaneously with formation of the O_W−P bond, one proton of the water molecule is transferred to the bridging oxygen, indicating that the bridging hydroxide serves as the general base to activate the attacking water. This attack results in the pentacoordinate intermediate shown in Figure 4. The barrier and reaction energy for this step are calculated to be 17.3 and 13.3 kcal/mol, respectively. The barrier for the base mechanism is thus significantly higher than the previously calculated barrier where the bridging hydroxide is the nucleophile [11.7 kcal/mol (*9*)]. These findings thus provide additional evidence that the bridging hydroxide acts as a nucleophile and not as a general base in the Zn/Zn−PTE reaction.

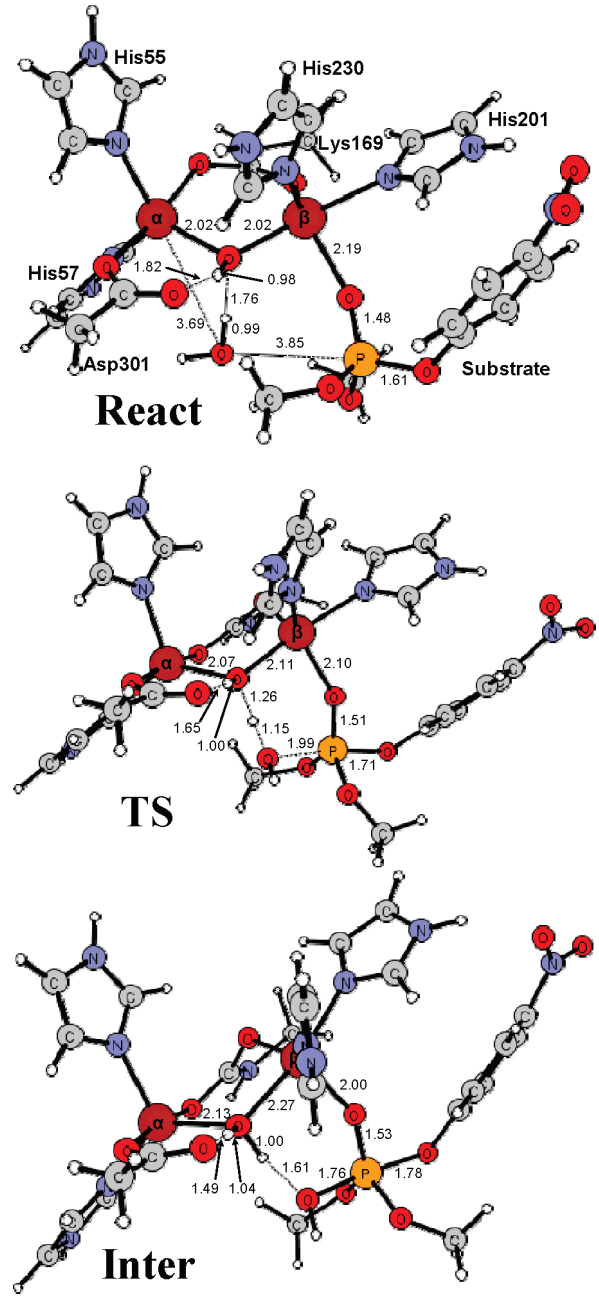

FIGURE 4: Optimized geometries of the Zn/Zn−PTE active site model with dimethyl 4-nitrophenyl phosphate and a water molecule bound (React), the transition state for the water attack on the phosphorus (TS), and the resulting pentacoordinate intermediate (Inter). Distances are in angstroms.

DISCUSSION

Enzyme−Product Complexes with PTE. The X-ray crystal structures of the diethyl phosphate product complex and an inhibitor complex with cacodylate have been determined with the phosphotriesterase from *P. diminuta*. The structures of these two complexes were determined in an attempt to provide experimental support for recent variations in the reaction mechanism that have been postulated for this enzyme (*10, 11*). With the diethyl phosphate product, the ligand is found bridging the two divalent cations as illustrated in Figure 3. The two metal ions are separated by a distance of 4.0 Å, where one of the negatively charged phosphate oxygens of the product is 2.1 Å from the α-metal ion while the other oxygen is 1.9 Å from the β-metal ion. There are no water molecules associated with either metal within a distance of 5.4 Å. The distances between the two divalent cations and bound ligands for the various complexes are compared in Figure 5. The symmetrical bridge observed in this complex differs from the prediction of this structure based upon the calculations of Wong and Gao (*10*). They have postulated that the diethyl phosphate product would be bound asymmetrically to the binuclear metal center with exclusive coordination to the β-metal ion and a metal−metal

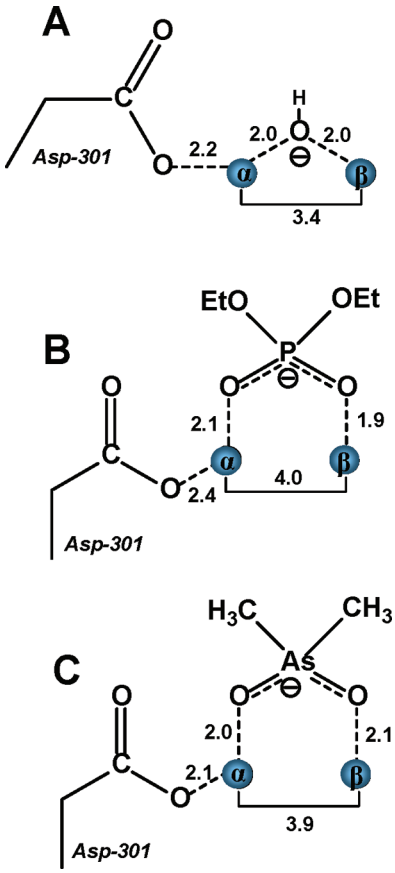

FIGURE 5: Schematic representations of the binuclear metal centers of the binuclear metal centers from the Co/Co−PTE hybrid in the presence and absence of diethyl phosphate and cacodylate. (A) Zn/Zn−PTE hybrid in the absence of added ligands (PDB entry 1HZY). (B) Co/Co−PTE hybrid in the presence of added diethyl phosphate (PDB entry 3CAK). (C) Co/Co−G60A PTE hybrid in the presence of cacodylate (PDB entry 2O4Q).

separation of 5.3 Å. It is unclear from the structure determined here whether the carboxylate side chain of Asp-301 is protonated. However, the nearest carboxylate oxygen of Asp-301 is found 2.4 Å from the α-metal ion in the diethyl phosphate complex compared with a distance of 2.5 Å in the unliganded complex (*8*). The structure of diethyl phosphate bound to PTE determined here is consistent with the complex proposed by Aubert et al. (*8*). There is no indication that the two divalent cations can be separated by a distance that approaches that of 5.3 Å predicted by Wong and Gao. The experimentally determined complex resembles that of a highly symmetric bridge with nearly equal distances between each metal ion and the nearest phosphate oxygen.

A nearly identical structure is observed for the G60A mutant in the complex with the cacodylate anion (Figure 3). The G60A mutant has kinetic constants nearly identical to those of the wild-type enzyme for the hydrolysis of paraoxon but is more stereoselective for the hydrolysis of substrates with larger substituents attached to the phosphorus core (*28*). Cacodylate is an analogue of the diethyl phosphate product since it bears a single negative charge within a tetrahedral architecture. The coordination geometry of this ligand with respect to the binuclear metal center is nearly symmetric with oxygen−metal distances of 2.0 and 2.1 Å for the α- and *β*-metal ions, respectively. There are no water molecules coordinated to either metal within 3.0 Å.

The coordination geometries of the diethyl phosphate and cacodylate bound to the binuclear metal center of PTE are not consistent with the mechanism for phosphotriester hydrolysis proposed by Jackson et al. (*11*). For the phosphotriesterase isolated from *A. radiobacter*, it has been postulated that the bridging hydroxide acts not as a nucleophile but as a general base in the abstraction of a proton from a water molecule coordinated to the α-metal ion. The primary experimental support for this conjecture stems from the determination of the structures of diethyl thiophosphate and dimethyl thiophosphate bound to the active site of the PTE from *A. radiobacter* (*11, 13*). These structures reveal a bridging complex for either thiophosphate product with the coordination of an additional bridging hydroxide. These complexes are consistent with the mechanism depicted in Scheme 3. However, to the best of our knowledge, there have been no crystal structures of PTE in which the α-metal ion is six-coordinate with an additional water molecule that could function as the primary nucleophile. Thus, experimental support for an additional water molecule that is activated by the bridging hydroxide is lacking. The identities of the metal ions bound to PTE from *A. radiobacter* are also different from those of the *P. diminuta* PTE. The structure of this enzyme was determined with Fe in the α-position and Zn in the *β*-position. Hexacoordinate zinc complexes are extremely rare, and thus, it seems quite unlikely that Zn/Zn−PTE from *P. diminuta* could function in the manner proposed by Ollis and co-workers. The DFT calculations presented here give further support to this conclusion. It was not possible to optimize a structure in which an additional water molecule is bound to the α-Zn atom and the barrier for the base mechanism is calculated to be significantly higher than that for the nucleophile mechanism.

Product Complexes in the Amidohydrolase Superfamily. X-ray crystal structures have been determined for other members of the amidohydrolase superfamily (*1*). It seems reasonable to assume that for those enzymes in this superfamily that contain a binuclear metal center many aspects of the chemical reaction mechanisms would be quite similar to one another. Structures of these enzymes, determined in the presence of their respective hydrolysis products, should illuminate whether the diethyl phosphate structure, determined for PTE, provides a common mechanistic or structural theme for the rest of the amidohydrolase superfamily.

Isoaspartyl dipeptidase (IAD) catalyzes the hydrolysis of amide bonds formed with the side chain carboxylate of aspartic acid (*29*). A 2.1 Å resolution structure of this enzyme has been determined in the presence of aspartate, the reaction product (*30*). A representation of the structure is illustrated in Figure 6 showing the bound aspartate. The carboxylate side chain is found bridging the two zinc atoms within the active site in a somewhat asymmetric arrangement. The two metal ions are separated by a distance of 3.8 Å. The carboxylate oxygen nearest the α-metal is separated by a distance of 2.8 Å, while the other oxygen is 2.3 Å from the *β*-metal ion. There are no other water molecules within 4.1 Å of either metal ion. A similar complex is also observed in the structure of acetate bound within the active site of D-aminoacylase (Figure 6). This enzyme catalyzes the hydrolysis of the amide bond of *N*-acetyl-D-amino acid derivatives (*31, 32*). This particular enzyme requires a divalent cation bound to the *β*-site but is less particular about

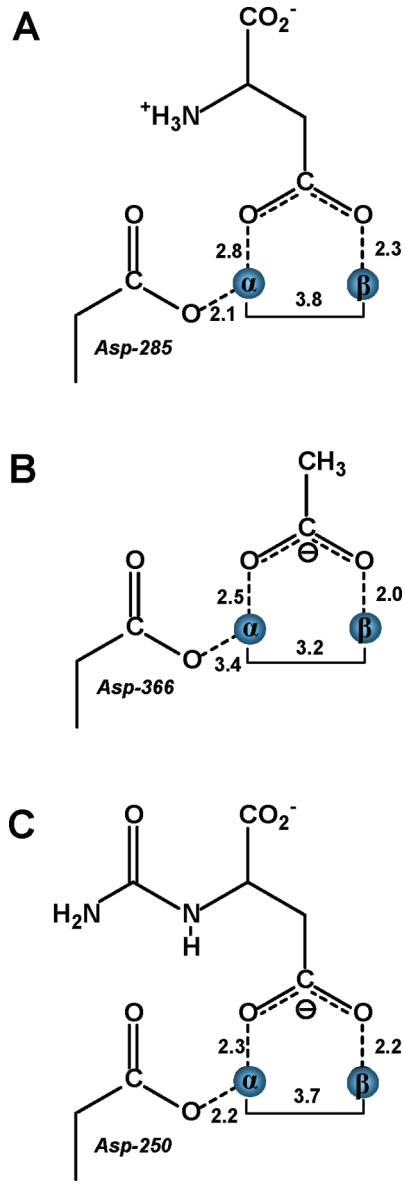

FIGURE 6: Schematic representations of the binuclear metal centers for isoaspartyl dipeptidase, D-aminoacylase, and dihydroorotase in the presence of bound reaction products. (A) Isoaspartyl dipeptidase in the presence of aspartic acid (PDB entry 1ONX). (B) D-Aminoacylase in the presence of acetate (PDB entry 1M7J). (C) Dihydroorotase in the presence of carbamoyl aspartate (PDB entry 1J79).

the requirement for the occupancy of the metal ion at the α-site. In any event, the coordination of acetate to the active site shows that the two metal ions are 3.2 Å from one another. One of the oxygens of the bound acetate is 2.5 Å from the α-metal, whereas the other oxygen is 2.0 Å from the β-metal. There are no other water molecules that are bound to either metal ion.

Dihydroorotase catalyzes the reversible interconversion of carbamoyl aspartate and dihydroorotate in the biosynthetic pathway for the assembly of pyrimidine nucleotides. When the structure of this enzyme was determined in the presence of added dihydroorotate, it was found, quite remarkably, that in one subunit of the dimer dihydroorotate was bound while in the adjacent subunit carbamoyl aspartate was bound. Thus, the structure of this enzyme−substrate/product complex provided a nearly unprecedented view of the reaction immediately before and after the chemical reaction had been catalyzed. In the complex with the bound carbamoyl aspartate, the two zinc atoms are separated by 3.7 Å. One of the carboxylate oxygens is 2.3 Å from the α-metal ion, while the other oxygen is 2.2 Å from the β-metal ion (*33*). Thus, the bridging complex is symmetric, and there are no other visible water molecules that could function as the nucleophile in the complex with dihydroorotate (Figure 6).

Conclusions. The structure of PTE from *P. diminuta* has been determined in the presence of the hydrolysis product diethyl phosphate and a product analogue, cacodylate. In either structure, the complex is formed as a bridging ligand between the two divalent cations in a symmetric orientation where the average oxygen−metal distance is 2.0 Å. The average metal−metal separation in this complex is 3.9 Å, compared with 3.4 Å in the unliganded complex. In either structure, there is no evidence for the additional binding of hydroxide to either of the two divalent cations. These results provide strong experimental support for the coordination geometry of the reaction product, originally postulated by Aubert et al. and illustrated in Scheme 2. The enzyme−product complex, predicted by Wong and Gao to be asymmetrically associated with only the β-metal ion coupled with a metal−metal separation of 5.3 Å, is not supported by these results (*10*). The structures presented in this paper are also at variance with the proposed mechanism postulated by Ollis and co-workers (*11, 13*). In the complex with diethyl phosphate, there is no evidence of the binding of an additional hydroxide as a bridging ligand between the two divalent cations. These results support the computational assessment of the reaction mechanism of PTE which concluded that the bridging hydroxide is sufficiently nucleophilic to attack the phosphorus center of organophosphate triester substrates (*9, 10, 34*). The formation of product complexes with the simultaneous complexation of hydroxide and product in the active site of PTE from *A. radiobacter* is likely the result of iron occupying the α-metal ion site of that enzyme.

SUPPORTING INFORMATION AVAILABLE

Electron density for cacodylate bound to the active site of G60A (Figure S1) and for diethyl phosphate bound to wild-type PTE (Figure S2A,B). This material is available free of charge via the Internet at http://pubs.acs.org.

REFERENCES

1. Seibert, C. M., and Raushel, F. M. (2005) Structural and catalytic diversity within the amidohydrolase superfamily. *Biochemistry 44*, 6383–6391.
2. Benning, M. M., Shim, H., Raushel, F. M., and Holden, H. M. (2001) High resolution X-ray structures of different metal-substituted forms of phosphotriesterase from *Pseudomonas diminuta*. *Biochemistry 40*, 2712–2722.
3. Donarski, W. J., Dumas, D. P., Heitmeyer, D. P., Lewis, V. E., and Raushel, F. M. (1989) Structure-activity relationships in the hydrolysis of substrates by the phosphotriesterase from *Pseudomonas diminuta*. *Biochemistry 28*, 4650–4655.
4. Dumas, D. P., Durst, H. D., Landis, W. G., Raushel, F. M., and Wild, J. R. (1990) Purification and properties of the phosphotriesterase for *Pseudomonas diminuta*. *Arch. Biochem. Biophys. 277*, 155–159.
5. Caldwell, S. R., Newcomb, J. R., Schlecht, K. A., and Raushel, F. M. (1991) Limits of diffusion in the hydrolysis of substrates by the phosphotriesterase from *Pseudomonas diminuta*. *Biochemistry 30*, 7438–7444.

6. Raushel, F. M., and and Holden, H. M. (2000) Phosphotriesterase: An enzyme in search of its natural substrate. *Adv. Enzymol. Relat. Areas Mol. Biol. 74*, 51–93.
7. Omburo, G. A., Kuo, J. M., Mullins, L. S., and Raushel, F. M. (1992) Characterization of the zinc binding site of bacterial phosphotriesterase. *J. Biol. Chem. 267*, 13278–13283.
8. Aubert, S. D., Li, Y., and Raushel, F. M. (2004) Mechanism for the hydrolysis of organophosphates by the bacterial phosphotriesterase. *Biochemistry 43*, 5707–5715.
9. Chen, S.-L., Fang, W.-H., and Himo, F. (2007) Theoretical study of the phosphotriesterase reaction mechanism. *J. Phys. Chem. B 111*, 1253–1255.
10. Wong, K.-Y., and Gao, J. (2007) The reaction mechanism of paraoxon hydrolysis by phosphotriesterase from combined QM/MM simulations. *Biochemistry 46*, 13352–13369.
11. Jackson, C. J., Foo, J. L., Kim, H. K., Carr, P. D., Liu, J. W., Salem, G., and Ollis, D. L. (2008) In crystallo capture of a Michaelis complex and product-binding modes of a bacterial phosphotriesterase. *J. Mol. Biol. 375*, 1189–1196.
12. Samples, C. R., Raushel, F. M., and DeRose, V. J. (2007) Activation of the binuclear metal center through formation of phosphotriesterase-inhibitor complexes. *Biochemistry 46*, 3435–3442.
13. Jackson, C., Kim, H. K., Carr, P. D., Liu, J. W., and Ollis, D. L. (2005) The structure of an enzyme-product complex reveals the critical role of a terminal hydroxide nucleophile in the bacterial phosphotriesterase mechanism. *Biochim. Biophys. Acta 1752*, 56–64.
14. Kuiper, J. M., Hulst, R., and Engberts, J. B. F. N. (2003) A selective and mild synthetic route to dialkyl phosphates. *Synthesis,* 695–698.
15. Otwinowski, Z., and Minor, W. (1997) Macromolecular crystallography, part A. In *Methods in Enzymology* (Carter, C. W., Jr., andSweet, R. M., Eds.) pp 307−326, Academic Press, New York.
16. Vagin, A., and Teplyakov, A. (1997) MOLREP: An automated program for molecular replacement. *J. Appl. Crystallogr. 30*, 1022–1025.
17. Lamzin, V. S., Wilson, K. S., and Perrakis, A. (2001) Crystallography of biological macromolecules. In *International Tables for Crystallography* (Rossmann, M. G., and Arnold, E., Eds.) pp 720−722, Kluwer Academic Publishers, Dordrecht, The Netherlands.
18. Emsley, P., and Cowtan, K. (2004) Coot: Model-building tools for molecular graphics. *Acta Crystallogr. D60* (Part 12, Special Issue 1), 2126–2132.
19. Murshudov, G. N., Vagin, A. A., and Dodson, E. J. (1997) Refinement of macromolecular structures by the maximum-likelihood method. *Acta Crystallogr. D53*, 240–255.
20. Becke, A. D. (1993) A new mixing of Hartree−Fock and local density-functional theories. *J. Chem. Phys. 98*, 1372–1377.
21. Becke, A. D. (1993) Density-functional thermochemistry III. The role of exact exchange. *J. Chem. Phys. 98*, 5648–5652.
22. Lee, C., Yang, W., and Parr, R. G. (1988) Development of the Colle-Salvetti correlation-energy formula into a functional of the electron density. *Phys. Rev. B 37*, 785–789.
23. Barone, V., and Cossi, M. (1998) Quantum calculation of molecular energies and energy gradients in solution by a conductor solvent model. *J. Phys. Chem. A 102*, 1995–2001.
24. Cammi, R., Mennucci, B., and Tomasi, J. (1999) Second-order Moller-Plesset analytical derivatives for the polarizable continuum model using the relaxed density approach. *J. Phys. Chem. A 103*, 9100–9108.
25. Klamt, A., and Schüürmann, G. (1993) COSMO: A new approach to dielectric screening in solvents with explicit expressions for the screening energy and its gradient. *J. Chem. Soc., Perkin. Trans. 2*, 799–800.
26. Tomasi, J., Mennucci, B., and Cammi, R. (2005) Quantum mechanical continuum solvation models. *Chem. Rev. 105*, 2999–3094.
27. Frisch, M. J., Trucks, G. W., Schlegel, H. B., et al. (2004) Gaussian 03, revision D.01, Gaussian, Inc., Wallingford, CT.
28. Chen-Goodspeed, M., Sogorb, M. A., Wu, F., Hong, S.-B., and Raushel, F. M. (2001) Structural determinants of the substrate and stereochemical specificity of phosphotriesterase. *Biochemistry 40*, 1325–1331.
29. Martí-Arbona, R., Fresquet, V., Thoden, J. B., Davis, M. L., Holden, H. M., and Raushel, F. M. (2005) Mechanism of the reaction catalyzed by isoaspartyl dipeptidase from *Escherichia coli*. *Biochemistry 44*, 7115–7124.
30. Thoden, J. B., Marti-Arbona, R., Raushel, F. M., and Holden, H. M. (2003) High-resolution X-ray structure of isoaspartyl dipeptidase from *Escherichia coli*. *Biochemistry 42*, 4874–4882.
31. Liaw, S.-H., Chen, S.-J., Ko, T.-P., Hsu, C.-S., Chen, C.-J., Wang, A. H.-J., and Tsai, Y.-C. (2003) Crystal structure of D-aminoacylase from *Alcaligenes faecalis* DA1. *J. Biol. Chem. 278*, 4957–4962.
32. Lai, W.-L., Chou, L.-Y., Ting, C.-Y., Kirby, R., Tsai, Y.-C., Wang, A. H.-J., and Liaw, S.-H. (2004) The functional role of the binuclear metal center in D-aminoacylase. *J. Biol. Chem. 279*, 13962–13967.
33. Thoden, J. B., Phillips, G. M., Neal, T. M., Raushel, F. M., and Holden, H. M. (2001) Molecular structure of dihydroorotase: A paradigm for catalysis through the use of a binuclear metal center. *Biochemistry 40*, 6989–6997.
34. Zheng, F., Znan, C.-G., and Ornstein, R. L. (2002) Theoretical determination of two structural forms of the active site in cadmium-containing phosphotriesterases. *J. Phys. Chem. B 106*, 717–722.

BI800971V